Rotational bands and signature inversion in odd-odd ^{172}Re

Y. H. Zhang,[1] M. Oshima,[2] Y. Toh,[2] X. H. Zhou,[1] M. Koizumi,[2] A. Osa,[2] A. Kimura,[2] Y. Hatsukawa,[2] T. Morikawa,[3] M. Nakamura,[3] M. Sugawara,[4] H. Kusakari,[5] T. Komatsubara,[6] K. Furuno,[6] H. L. Wang,[1] P. Luo,[1] C. S. Wu,[7] and F. R. Xu[7]
[1]*Institute of Modern Physics, Chinese Academy of Sciences, Lanzhou 730000, People's Republic of China*
[2]*Japan Atomic Energy Research Institute, Tokai-mura, Ibaraki 319-1195, Japan*
[3]*Department of Physics, Kyushu University, Fukuoka 812-81, Japan*
[4]*Chiba Institute of Technology, Narashino, Chiba 275-0023, Japan*
[5]*Chiba University, Inage-ku, Chiba 263-8512, Japan*
[6]*Institute of Physics and Tandem Accelerator Center, University of Tsukuba, Ibaraki 305-8577, Japan*
[7]*Department of Technical Physics and MOE Key Laboratory, Peking University, Beijing 100871, People's Republic of China*
(Received 6 March 2003; published 21 November 2003)

High-spin states in the odd-odd ^{172}Re have been investigated via the ^{149}Sm(^{27}Al, $4n\gamma$)^{172}Re reaction through excitation functions, x-γ and γ-γ coincidence measurements. A level scheme consisting of three rotational bands has been identified for the first time extending the high-spin studies of $A\sim160$ odd-odd nuclei to the currently lightest rhenium isotope. The three bands have been assigned to be built on the $\pi h_{11/2}\otimes\nu i_{13/2}$, $\pi h_{9/2}\otimes\nu i_{13/2}$, and $\pi 1/2^-[541]\otimes\nu 1/2^-[521]$ configurations according to their rotational properties in quasiparticle alignments, signature splitting, in-band $B(M1)/B(E2)$ ratios, level spacing systematics, band crossing frequencies, as well as the existing knowledge in neighboring nuclei. Low-spin signature inversion has been confirmed in the first two bands due to the observation of signature crossing at high-spin states. The general features of inversion phenomenon in the semidecoupled bands are presented and discussed with reference to theoretical calculations of two quasiparticle plus rotor model including p-n interactions.

DOI: 10.1103/PhysRevC.68.054313 PACS number(s): 21.10.Re, 23.20.Lv, 27.70.+q

I. INTRODUCTION

The invariance of the intrinsic Hamiltonian of an axially deformed nucleus with respect to 180° rotation around a principal axis gives rise to the conserved quantum number of signature α. Consequently, a $\Delta I=1$ collective rotational band in odd-A and odd-odd nuclei can be classified as two $\Delta I=2$ branches characterized by different signatures, $\alpha=\pm1/2$ in odd nuclei and $\alpha=0$ or 1 in odd-odd nuclei. For each signature branch, the spins of the levels are defined by $I=\alpha$ mod 2. Usually, one branch is favored, i.e., lower in energy, whereas the other one is unfavored. The energy difference between the two branches is called the signature splitting which is expected to increase gradually with rotational frequency due to Coriolis interaction. For an odd-A nucleus, the expected favored (unfavored) $\Delta I=2$ branch corresponds to a so-called favored (unfavored) signature defined by $\alpha_f=1/2\times(-1)^{j-1/2}$ [$\alpha_{uf}=1/2\times(-1)^{j+1/2}$] [1], where j is the angular momentum of the subshell associated with the valence nucleon. Theoretically, signature α is an additive quantity, thus the energetically favored band of a two-quasiparticle configuration is expected to have a favored signature determined by $\alpha_f=1/2\times(-1)^{j_\nu-1/2}+1/2\times(-1)^{j_\pi-1/2}$, where ν and π represent the neutron and the proton, respectively. For the odd-odd nuclei in $A\sim160$ mass region, however, this rule is broken in a number of two-quasiparticle bands built on the $\pi h_{11/2}\otimes\nu i_{13/2}$ and $\pi h_{9/2}\otimes\nu i_{13/2}$ configurations [2–5], that is, the expected favored branch lies higher in energy than the unfavored one at low and medium spins. This is known as the low-spin signature inversion [6]. Such signature inversion phenomena have also been observed in certain bands of odd-odd nuclei in other mass regions. These include the $\pi g_{9/2}\otimes\nu g_{9/2}$ bands of $A\sim80$ nuclei, the $\pi h_{11/2}\otimes\nu h_{11/2}$ bands of $A\sim130$ nuclei (see Ref. [7], and references therein), and more recently the $\pi i_{13/2}\otimes\nu i_{13/2}$ bands of $A\sim180$ nuclei [8–11]. Several theoretical attempts have been made suggesting that the triaxiality [6], proton-neutron (p-n) interaction [4,12,13], band crossings [14], band mixing [15], quadrupole pairing [16], and the combined effects [17] could be possible reasons for the inversion phenomenon. However, no conclusive explanation has been made so far. From systematic analyses for the bands of $\pi h_{11/2}\otimes\nu i_{13/2}$ configuration [2–4,7], one has found that the critical spin I_c (called the signature crossing spin hereafter), at which two signature branches cross with each other, *increases* (*decreases*) regularly with increasing two protons (neutrons) for a chain of isotones (isotopes). However, an opposite trend has been observed for the $\pi h_{9/2}\otimes\nu i_{13/2}$ bands, i.e., I_c decreases (increases) with increasing two protons (neutrons) for a chain of isotones (isotopes) [4,5]. To extend the systematics to a wide range of nuclei and investigate the inversion phenomenon, we undertook an experiment on ^{172}Re.

The spin and parity of 5^+ were tentatively assigned to the ground state of ^{172}Re previously according to its intense β^+/EC feeding to the 4^+ and 6^+ rotational levels in ^{172}W [18]. The high-spin states in ^{172}Re have not been studied so far. The present work extends high-spin studies of odd-odd $A\sim160$ nuclei to the lightest rhenium isotope investigated to date. In this paper, we report on the first observation of three rotational bands in ^{172}Re. The configurations can be assigned as $\pi h_{11/2}(9/2^-[514])\otimes\nu i_{13/2}$, $\pi h_{9/2}(1/2^-[541])\otimes\nu i_{13/2}$, and $\pi h_{9/2}(1/2^-[541])\otimes\nu 1/2^-[521]$, respectively. The first two bands present low-spin signature inversion. The spin and configuration assignments of these bands have been made on

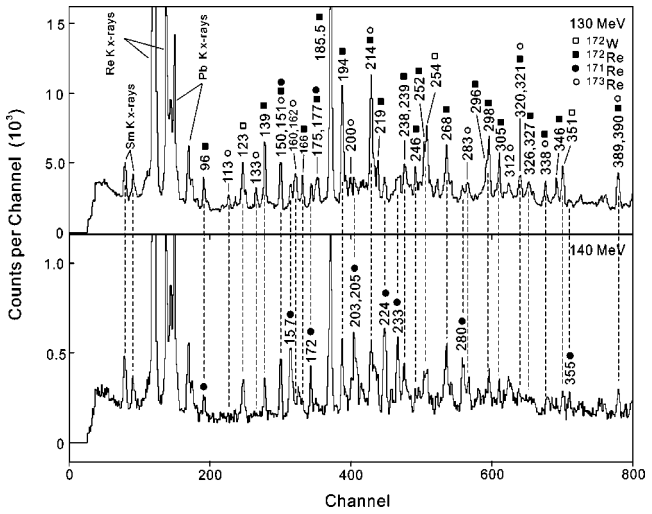

FIG. 1. Re *K* x-ray gated spectra at 130-MeV (upper panel) and 140-MeV (lower panel) beam energies.

the basis of analyses of quasiparticle alignments, in-band electromagnetic transition properties, level spacing systematics, and systematic features of signature splitting. General features of signature inversion in the $\pi h_{9/2}(1/2^-[541]) \otimes \nu i_{13/2}$ bands are presented and the possible reasons are discussed qualitatively with reference to the two quasiparticle plus rotor model calculations with *p-n* residual interactions included.

II. EXPERIMENTAL DETAILS AND RESULTS

A. Measurements

In order to obtain information on the high-spin states in ^{172}Re, we have carried out a standard in-beam γ-ray spectroscopy experiment at the Japan Atomic Energy Research Institute (JAERI). An enriched ^{149}Sm target of 2.1 mg/cm^2 thickness with a 5.5 mg/cm^2 Pb backing was bombarded by an ^{27}Al beam delivered from the JAERI tandem accelerator. The high-spin states in odd-odd ^{172}Re were populated via the ^{149}Sm(^{27}Al, $4n\gamma$)^{172}Re reaction. A BGO-HPGe array GEMINI [19] was used to detect the γ rays. The array consisted of 12 large volume HPGe detectors with BGO anti-Compton shields. The energy and efficiency calibrations were made using ^{60}Co, ^{133}Ba, and ^{152}Eu standard sources. Typical energy resolutions were about 2.0$\sim$2.5 keV at full width at half maximum for the 1332.5-keV line.

The in-beam γ rays belonging to ^{172}Re were identified by measuring an excitation function at beam energies of 130, 135, 140, and 150 MeV. The γ-ray spectra in this experiment were very complex; the photon peaks were often doublets or contaminated by the γ rays from other reaction channels. We therefore used coincidence mode in the excitation function measurements. At each beam energy, about 10×10^6 γ-γ coincidence events were accumulated and sorted on-line into a symmetric E_γ-E_γ matrix of $4k\times4k$ size. The Re *K* x-ray gated γ-ray spectra were projected and analyzed during experiment. The intensities of known γ rays from ^{173}Re (^{171}Re) decrease (increase) apparently with increasing beam energy, whereas numerous unknown γ rays were found to have

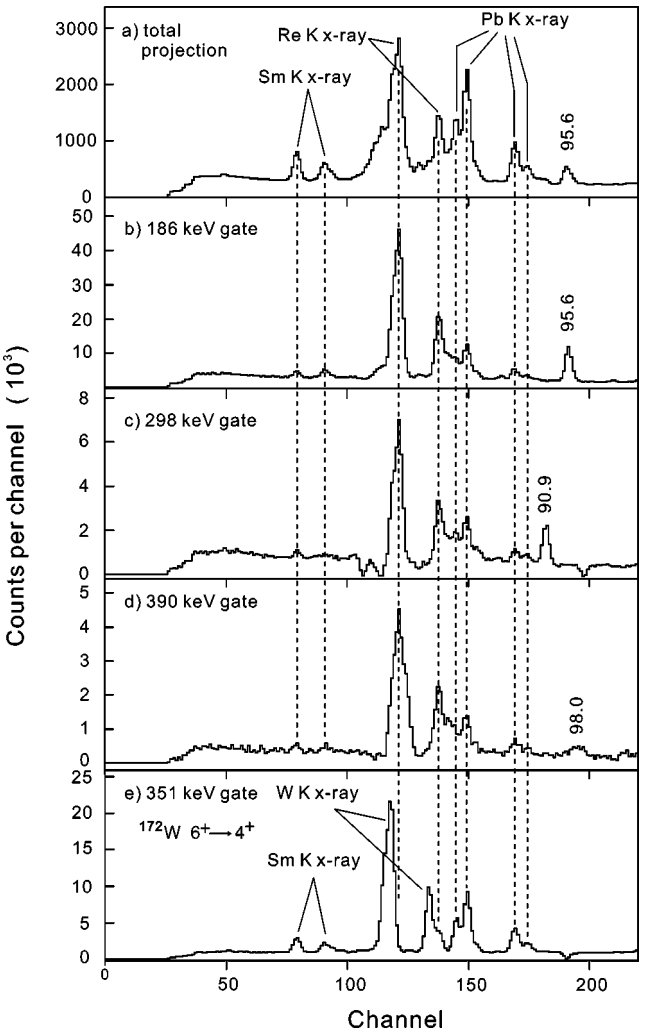

FIG. 2. Low-energy portions of (a) total projection, (b) 186-keV, (c) 298-keV, (d) 390-keV, and 351-keV ($6^+\rightarrow4^+$ transition in ^{172}W) gated spectra at a beam energy of 130 MeV.

higher or comparable intensities to those from ^{173}Re and ^{171}Re at beam energies of 130 MeV through 140 MeV. This can be seen in the Re *K* x-ray gated spectra presented in Fig. 1, where the γ rays emitted from ^{173}Re (113-, 133-, 160-, 162-keV lines [20]) have been observed at 130-MeV beam energy (upper panel) whereas the γ rays from ^{171}Re (indicated by the filled circles [20]) are much enhanced at the beam energy of 140 MeV (lower panel). Low-energy portions of coincidence spectra obtained by setting gates on 186-, 298-, 390-keV lines are displayed in Fig. 2 together with those of total projection and the 351-keV ($6^+\rightarrow4^+$ transition in ^{172}W) gated spectra for comparison; the Re *K* x-ray can be well separated from that of tungsten indicating that the 186-, 298-, and 390-keV lines and the associated cascade transitions shown in Fig. 3 are from a rhenium isotope. It should be noted that the relatively intense γ rays in this experiment were from the fusion-evaporation residues of ^{171,172,173}Re, ^{171,172}W, and ^{169}Ta corresponding to 5*n*, 4*n*, 3*n*, 4*np*, 3*np*, and α3*n* evaporation channels, respectively. Since the high-spin level schemes for ^{171,173}Re [20], ^{171,172}W [21], and ^{169}Ta [22] had been well established, γ-ray assignment

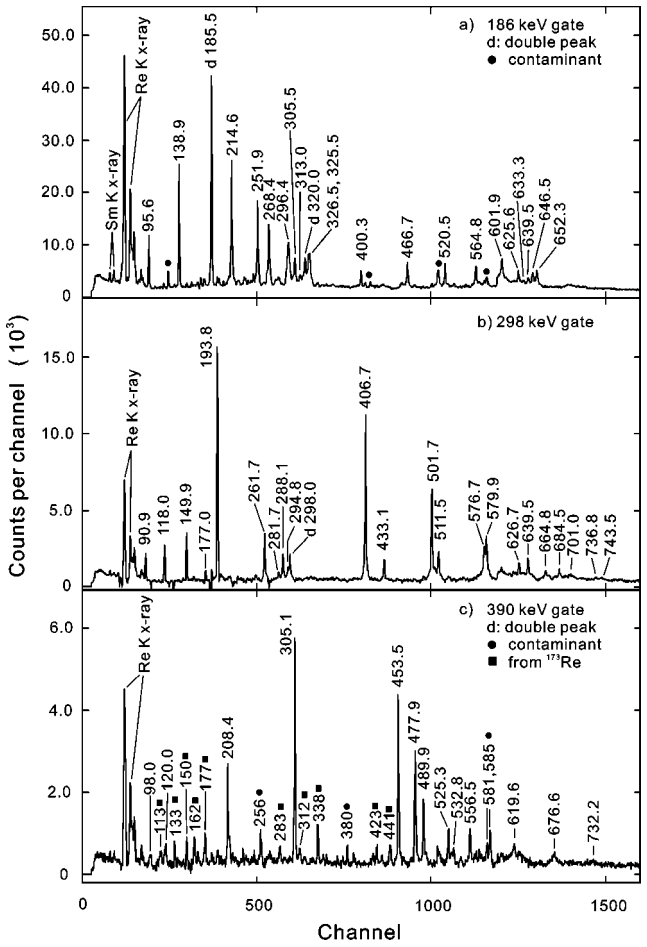

FIG. 3. Selected coincidence spectra for bands 1, 2, and 3.

in ^{172}Re could be carried out using this information and the measurements of excitation functions (Fig. 1) and x-γ coincidence data (Fig. 2).

A beam energy of 130 MeV was used for γ-γ coincidence measurements. About 250×10^6 coincidence events were accumulated and sorted into a symmetric E_γ-E_γ matrix of $4k\times4k$ size for off-line analysis. To obtain the multipolarity information of emitting γ rays, the detectors were divided into three groups positioned at ±32° (±148°), ±58° (±122°), and ±90° with respect to the beam direction. Two nonsymmetrized matrices were constructed from the coincidence data: one matrix with detectors at $\theta_1=\pm32°$ (or ±148°) and another one with $\theta_2=\pm90°$ against those at all angles. From these two matrices, the angular distribution ratios defined as $R_{AD}(\gamma)=I_\gamma(\theta_1)/I_\gamma(\theta_2)$ were extracted from the γ-ray intensities $I_\gamma(\theta_1)$ and $I_\gamma(\theta_2)$ in the coincidence spectra gated by γ transitions of any multipolarities (it is supposed that the angular distribution effects of the gating γ transitions could be neglected in the nonsymmetrized matrices). Usually a single gate was used for strong peaks. For some weak transitions, the sum-gated spectra were used in order to get high statistics. In the present geometry, stretched quadrupole transitions were adopted if $R_{AD}(\gamma)$ values were larger than unity [an average value of $R_{AD}(\gamma)=1.30\pm0.15$ was obtained for the known $E2$ transitions in ^{171,172}W], and dipole transitions were assumed if $R_{AD}(\gamma)$'s were significantly less than 1.0.

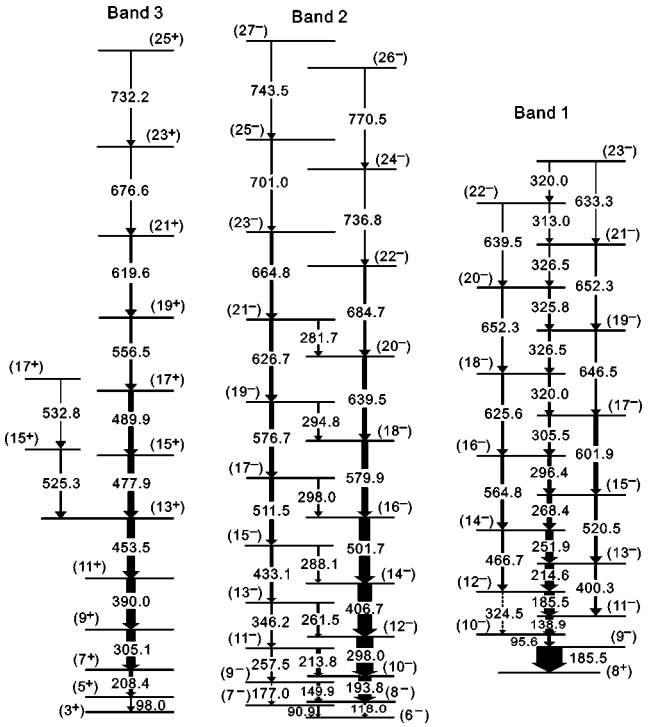

FIG. 4. Partial level scheme of ^{172}Re deduced from the present work.

B. Level scheme

From detailed analyses of the coincidence data, a partial level scheme of ^{172}Re has been established by the present work and is shown in Fig. 4. Typical coincidence spectra are presented in Fig. 3, showing the quality of the data. The γ-transition energies in the level scheme are within an uncertainty of 0.5 keV, and the ordering of the transitions within a band is established on the basis of γ-γ coincidence relationships, γ-ray energy sums, and γ-ray relative intensities. No linking transitions have been observed among the three bands observed. The relative spins within a band are proposed in terms of the measured AD ratios of emitting γ rays.

The 185.5-keV line was very strong in the total projection spectrum. It coincides with itself and all the γ rays in band 1 [see Fig. 3(a)] indicating that 185.5-keV line is a double peak: one 185.5-keV γ ray belongs to the in-band $\Delta I=1$ transition and the other corresponds to the deexcitation of the band head via most likely an $E1$ radiation. Indeed, the AD ratio using 400-keV gate was determined to be $R_{AD}(185.5\text{ keV})=0.85(8)$ indicating that the 185.5-keV line depopulating the band hand has $\lambda=1$ multipole order. On the other hand, the intensity ratios, $R=I_\gamma(139\text{ keV})/I_\gamma(95.6\text{ keV})=1.98(36)$ and $R=I_\gamma(139\text{ keV})/I_\gamma(185.5\text{ keV})=0.338(48)$, have been extracted using the 400-keV gated spectrum. Assuming that the 139-keV line is an in-band $M1$ transition, the total conversion coefficient has been calculated to be $\alpha_T^{th}(139\text{ keV};M1)=2.08$. Then the experimental conversion coefficients for 95.6- and 185.5-keV transitions were deduced through the use of intensity balance, i.e., $\alpha_T^{\text{expt}}(95.6\text{ keV})=5.1(9)$ and $\alpha_T^{\text{expt}}(185.5\text{ keV})=4.2(6)\times10^{-2}$ (note $\alpha_T^{\text{expt}}=[1+\alpha_T^{th}(139\text{ keV})]\times R-1$). These values are consistent with the theoretical calculations of

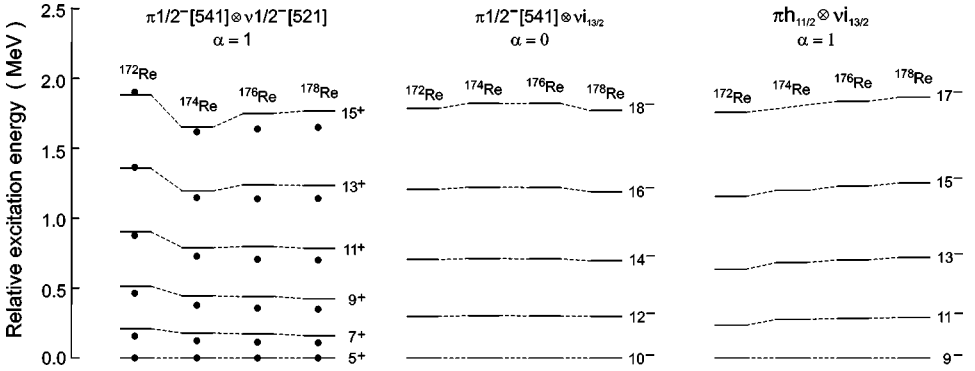

FIG. 5. Level spacing systematics in $^{172-178}$Re for the three configurations indicated in the figure. The data are from Refs. [4,24,25].

α_T^{th}(95.6 keV; $M1$)=6.1 and α_T^{th}(185.5 keV; $E1$)=7.9×10^{-2}. Therefore we assign the 95.6-keV line to be an in-band $M1$ transition, and the 185.5-keV line to deexcite the band head (9^-) and feed most probably to an 8^+ state. The 320- and 652-keV double peaks and the 326-keV triple lines were identified and assigned in band 1 according to their coincidence relationships and energy sums.

The branching ratios, defined as

$$\lambda = \frac{T_\gamma(I \to I-2)}{T_\gamma(I \to I-1)}, \tag{1}$$

were extracted for most transitions. Here $T_\gamma(I\to I-2)$ and $T_\gamma(I\to I-1)$ are the γ-ray intensities of the $\Delta I=2$ and $\Delta I=1$ transitions, respectively. These intensities were deduced from a coincidence spectrum gated by the transition above the state of interest. The branching ratios were used to extract the reduced transition probability ratios, which are defined as

$$\frac{B(M1, I \to I-1)}{B(E2, I \to I-2)} = 0.697\frac{[E_\gamma(I \to I-2)]^5}{[E_\gamma(I \to I-1)]^3}\frac{1}{\lambda}\frac{1}{1+\delta^2}\left(\frac{\mu_N^2}{e^2 b^2}\right), \tag{2}$$

where δ is the $E2/M1$ mixing ratio for the $\Delta I=1$ transitions, and $E_\gamma(I\to I-1)$ and $E_\gamma(I\to I-2)$ are the $\Delta I=1$ and $\Delta I=2$ transition energies, respectively. In the calculation, δ has been set to zero, since no mixing ratio could be deduced from the present data. Thus the experimental $B(M1)/B(E2)$ ratios extracted here should be regarded as upper limits.

The absolute excitation energies of these bands presented in Fig. 4 are not known since neither interband connections nor connections from these bands to the ground states could be established. This prevents us from making firm spin and parity assignments using spectroscopic methods. The spin and parity given in Fig. 4 rely only on the band structure systematics in odd-odd nuclei of this mass region. The three bands observed in ^{172}Re can be framed, as classified by Kreiner *et al.* [23], into compressed (band 1), semidecoupled (band 2), and doubly decoupled (band 3) bands built on the $\pi h_{11/2}(9/2^-[514])\otimes\nu i_{13/2}$, $\pi h_{9/2}(1/2^-[541])\otimes\nu i_{13/2}$, and $\pi h_{9/2}(1/2^-[541])\otimes\nu 1/2^-[521]$ configurations, respectively (configuration assignments will be further discussed in Sec. III). A comparison of the level energies in the three corresponding bands of odd-odd $^{172-178}$Re [24,4,25] is shown in Fig. 5 where the level spins in the $\pi h_{11/2}(9/2^-[514])\otimes\nu i_{13/2}$ and $\pi h_{9/2}(1/2^-[541])\otimes\nu i_{13/2}$ bands of ^{178}Re have been changed [4] adding one unit to the values assigned in Ref. [25]. The $I=(9^-)$, (10^-), and (5^+) states are set to 0 keV for bands 1, 2, and 3, such that the relative level energies for higher-lying states may be compared. The excitation energies of corresponding ground-state bands in the even-even $^{170-176}$W are also plotted as filled circles in Fig. 5. The smooth trends for the $\pi h_{11/2}(9/2^-[514])\otimes\nu i_{13/2}$ (band 1) and $\pi h_{9/2}(1/2^-[541])\otimes\nu i_{13/2}$ (band 2) structures are observed in the energy levels using our proposed level spins in ^{172}Re. The doubly decoupled bands are expected to follow the level spacings of the ground-state bands of the corresponding even-even cores [26]. Our spin assignment for band 3 leads to an increase of level energies in ^{172}Re (see left part of Fig. 5); this could be due to the similar behavior of ground-state band in the even-even ^{170}W. The level spacing systematics has been frequently used for spin assignments in odd-odd nuclei in different mass region [3,27,28]. This empirical method fixes the level spin within one unit although the validity needs further investigation.

The 139-, 407-, and 390-keV lines were less contaminated, and their relative intensities could be extracted in the total projection spectrum. Most of the γ-ray relative intensities in each band were extracted from the spectra gated on the bottom transitions. For some weak or heavily contaminated γ rays, only upper or lower limits are given based on their intensity balance. The γ-ray energies, spin and parity assignments, relative γ-ray intensities, branching ratios, extracted $B(M1)/B(E2)$ values, and the R_{AD} ratios are presented in Table I, grouped in sequences for each band.

III. DISCUSSIONS

A. Configuration assignments

The $\pi 1/2^-[541]$, $\pi 9/2^-[514]$, and $\pi 5/2^+[402]$ bands in ^{171,173}Re [20] and the $\nu i_{13/2}$ bands in ^{171,173}W [21,29] are strongly populated in heavy-ion-induced fusion-evaporation reactions. Thus, the two-quasiparticle bands built on the $\pi h_{11/2}(9/2^-[514])\otimes\nu i_{13/2}$ and $\pi h_{9/2}(1/2^-[541])\otimes\nu i_{13/2}$ configurations are expected, *a priori*, to be favorably populated in the (HI, xn) reactions because they also involve high-j orbitals. These two configurations correspond most probably to band 1 **(**$\pi h_{11/2}(9/2^-[514])\otimes\nu i_{13/2}$**)** and band 2 **(**$\pi h_{9/2}(1/2^-[541])\otimes\nu i_{13/2}$**)** observed in ^{172}Re. It has been known that the $\pi h_{11/2}(9/2^-[514])\otimes\nu i_{13/2}$ band exhibits two

TABLE I. γ-ray transition energies, spin and parity assignments, γ intensities, branching ratios, AD ratios, and extracted $B(M1)/B(E2)$ ratios in ^{172}Re.

E_γ (keV)[a]	$J_i^\pi \rightarrow J_f^\pi$[b]	I_γ[c]	λ[d]	R_{AD} ratio	$B(M1)/B(E2)$[e]
Band 1					
185.5[f]		$\geqslant$2500		0.85(8)	
95.6	$(10^-)\rightarrow(9^-)$	$\geqslant$225		1.50(15)	
138.9	$(11^-)\rightarrow(10^-)$	565		1.20(12)	
185.5	$(12^-)\rightarrow(11^-)$	$\leqslant$1016		0.97(10)	
400.3	$(13^-)\rightarrow(11^-)$	176		1.27(15)	
214.6	$(13^-)\rightarrow(12^-)$	640	0.39(4)	1.09(10)	1.86(20)
466.7	$(14^-)\rightarrow(12^-)$	200		1.29(13)	
251.9	$(14^-)\rightarrow(13^-)$	540	0.59(6)	0.98(10)	1.65(16)
520.5	$(15^-)\rightarrow(13^-)$	240		1.10(10)	
268.4	$(15^-)\rightarrow(14^-)$	360	0.79(8)	1.30(15)	1.75(18)
564.8	$(16^-)\rightarrow(14^-)$	220		1.50(20)	
296.4	$(16^-)\rightarrow(15^-)$	243	0.93(9)	0.98(10)	1.65(17)
601.9	$(17^-)\rightarrow(15^-)$	300			
305.5	$(17^-)\rightarrow(16^-)$	220	1.42(15)		1.36(15)
625.6	$(18^-)\rightarrow(16^-)$	210			
320.0	$(18^-)\rightarrow(17^-)$	220	0.94(10)		2.17(30)
646.5	$(19^-)\rightarrow(17^-)$	160			
326.5	$(19^-)\rightarrow(18^-)$	200			
652.3	$(20^-)\rightarrow(18^-)$	135			
325.8	$(20^-)\rightarrow(19^-)$	150			
652.3	$(21^-)\rightarrow(19^-)$	135			
326.5	$(21^-)\rightarrow(20^-)$	100			
639.5	$(22^-)\rightarrow(20^-)$	120			
313.0	$(22^-)\rightarrow(21^-)$	86			
633.3	$(23^-)\rightarrow(21^-)$	50			
320.0	$(23^-)\rightarrow(22^-)$	70			
Band 2					
90.9	$(7^-)\rightarrow(6^-)$	$\geqslant$137		0.97(20)	
118.0	$(8^-)\rightarrow(6^-)$	$\geqslant$175		1.80(30)	
177.0	$(9^-)\rightarrow(7^-)$	74			
149.9	$(9^-)\rightarrow(8^-)$	270	0.25(3)	0.75(8)	0.14(2)
193.8	$(10^-)\rightarrow(8^-)$	946		1.53(15)	
257.5	$(11^-)\rightarrow(9^-)$	114		1.36(15)	
213.8	$(11^-)\rightarrow(10^-)$	302	0.51(5)	0.64(10)	0.16(2)
298.0	$(12^-)\rightarrow(10^-)$	1210		1.31(13)	
346.2	$(13^-)\rightarrow(11^-)$	142		1.20(15)	
261.7	$(13^-)\rightarrow(12^-)$	185	0.76(7)	0.65(10)	0.25(3)
406.7	$(14^-)\rightarrow(12^-)$	1000		1.47(15)	
433.1	$(15^-)\rightarrow(13^-)$	216		1.32(13)	
288.1	$(15^-)\rightarrow(14^-)$	157	1.68(20)	0.48(10)	0.24(3)
501.7	$(16^-)\rightarrow(14^-)$	786		1.30(15)	
511.5	$(17^-)\rightarrow(15^-)$	$\geqslant$296			
298.0	$(17^-)\rightarrow(16^-)$	$\leqslant$150			
579.9	$(18^-)\rightarrow(16^-)$	485		1.38(15)	
576.7	$(19^-)\rightarrow(17^-)$	$\geqslant$344		1.38(15)	
294.8	$(19^-)\rightarrow(18^-)$	$\geqslant$80			
639.5	$(20^-)\rightarrow(18^-)$	320			
626.7	$(21^-)\rightarrow(19^-)$	191			
281.7	$(21^-)\rightarrow(20^-)$	50			
684.5	$(22^-)\rightarrow(20^-)$	163			
664.8	$(23^-)\rightarrow(21^-)$	$\geqslant$225			
736.8	$(24^-)\rightarrow(22^-)$	80			
701.0	$(25^-)\rightarrow(23^-)$	$\geqslant$130			
770.5	$(26^-)\rightarrow(24^-)$	$\geqslant$40			
743.5	$(27^-)\rightarrow(25^-)$	$\geqslant$60			
Band 3					
98.0	$(5^+)\rightarrow(3^+)$	$\geqslant$100			
208.4	$(7^+)\rightarrow(5^+)$	$\geqslant$283		1.48(15)	
305.1	$(9^+)\rightarrow(7^+)$	636		1.38(10)	
390.0	$(11^+)\rightarrow(9^+)$	615		1.35(10)	
453.5	$(13^+)\rightarrow(11^+)$	821		1.35(10)	
525.3	$(15^+)\rightarrow(13^+)$	160		1.30(10)	
532.8	$(17^+)\rightarrow(15^+)$	80			
477.9	$(15^+)\rightarrow(13^+)$	430		1.28(10)	
489.9	$(17^+)\rightarrow(15^+)$	360		1.30(10)	
556.5	$(19^+)\rightarrow(17^+)$	220		1.20(20)	
619.6	$(21^+)\rightarrow(19^+)$	180			
676.6	$(23^+)\rightarrow(21^+)$	120			
732.2	$(25^+)\rightarrow(23^+)$	70			

[a]Uncertainties are within 0.5 keV.
[b]See text for details about the spin and parity assignments.
[c]Uncertainties between 5 and 30%.
[d]Branching ratio: $T_\gamma(I\rightarrow I-2)/T_\gamma(I\rightarrow I-1)$, $T_\gamma(I\rightarrow I-2)$, and $T_\gamma(I\rightarrow I-1)$ are the relative γ intensities of the $E2$ and $M1$ transition depopulating the level I, respectively.
[e]Extracted from the branching ratios assuming $\delta^2=0$.
[f]γ-ray deexciting the band head.

typical features of small signature splitting **(**associated with the $\pi h_{11/2}(9/2^-[514])$ proton**)** and intense in-band $\Delta I=1$ transitions. This is due to its high-K and large-g_K values; both factors enhance the in-band $\Delta I=1$ transition strength. The analyses of in-band electromagnetic transition properties, as we shall present in Sec. III C, demonstrate that band 1 has the largest $B(M1)/B(E2)$ ratios, suggesting strongly that it is built on the $\pi h_{11/2}(9/2^-[514])\otimes\nu i_{13/2}$ configuration.

Band 2 shows the irregular in-band $\Delta I=1$ transition energies (e.g., signature splitting) already exist at low spins; this is a common feature [30] of so-called semidecoupled structures in odd-odd nuclei in this mass region. As noted in Ref. [16], the signature splitting in a two-quasiparticle band of odd-odd nuclei depends on the orbital which has smaller signature splitting. For the $\pi h_{9/2}(1/2^-[541])\otimes\nu i_{13/2}$ structure, the quasiproton occupies only the signature-favored orbital (in the terminology of cranked shell model [31]) because here the low-Ω, high-j orbital $h_{9/2}(1/2^-[541])$ has large signature splitting, while both favored and unfavored orbitals can be occupied by the $i_{13/2}$ quasineutron. Thus the signature splitting in the $\pi h_{9/2}(1/2^-[541])\otimes\nu i_{13/2}$ band may originate from the $i_{13/2}$ neutron orbital, and its amplitude could be comparable to that in the $\nu i_{13/2}$ bands of neighboring odd-N nuclei. This is the case of band 2 observed in ^{172}Re; one can

TABLE II. Parameters used in the calculations of $B(M1)/B(E2)$ ratios and alignments i_x in the three bands in ^{172}Re and the associated odd-mass neighbors.

Nucleus	Band	α	$J_0/\hbar^2$ (MeV^{-1})	$J_1/\hbar^4$ (MeV^{-3})	i_x ($\hbar$)	$\hbar\omega_c$ (MeV)	Expected crossing	g_Ω
^{170}W	gsb	0	16.4	236.2	0	0.25	*AB*	
^{171}W	$5/2^+[652](i_{13/2})$	+1/2	22.9	148.2	5.1	0.31	*BC*	−0.25
^{171}W	$5/2^+[652](i_{13/2})$	−1/2	20.8	139.2	4.3	0.35	*AD*	−0.25
^{173}W	$1/2^-[521]$	−1/2	32.2	406.9	0.5	∼0.25	*AB*	0.71
^{171}Re	$9/2^-[514](h_{11/2})$	−1/2	9.0	241.5	2.5	0.24	*AB*	1.29
^{171}Re	$9/2^-[514](h_{11/2})$	+1/2	9.0	241.5	2.5	0.24	*AB*	1.29
^{171}Re	$1/2^-[541](h_{9/2})$	+1/2	27.8	84.9	2.6	0.27	*AB*	0.83
^{172}Re	$\pi h_{11/2}\otimes\nu i_{13/2}$	1	18.0	170.2	6.6	0.30	*BC*	
^{172}Re	$\pi h_{11/2}\otimes\nu i_{13/2}$	0	18.0	170.2	6.6	0.30	*BC*	
^{172}Re	$\pi h_{9/2}\otimes\nu i_{13/2}$	1	22.4	176.7	7.8	⩾0.37	*BC*	
^{172}Re	$\pi h_{9/2}\otimes\nu i_{13/2}$	0	21.9	135.0	7.8	⩾0.37	*AD*	
^{172}Re	$\pi h_{9/2}\otimes\nu 1/2^-[521]$	1	33.6	157.1	2.8	0.24	*AB*	

see significant signature splitting by observing simply the irregular in-band $\Delta I=1$ transition energies. Another typical feature for the $\pi h_{9/2}(1/2^-[541])\otimes\nu i_{13/2}$ bands is the appearance of low-spin signature inversion which will be discussed in Sec. III D. In view of these, we assign the configuration of $\pi h_{9/2}(1/2^-[541])\otimes\nu i_{13/2}$ for band 2.

Band 3 consists of a cascade of $\Delta I=2$ transitions, and is considered to be the doubly decoupled band [23,30] based on the $\pi h_{9/2}(1/2^-[541])\otimes\nu 1/2^-[521]$ configuration. This structure involves both a proton and a neutron predominantly in $\Omega=1/2$ orbitals. Because of large signature splitting, the unfavored $\Delta I=2$ transition sequence is usually difficult to observe. The transition energies follow the level spacings of the ground-state band of the corresponding even-even ^{170}W core (see Fig. 5). This is a typical feature of doubly decoupled bands built on the $\pi h_{9/2}(1/2^-[541])\otimes\nu 1/2^-[521]$ configuration [26]. Similar bands have been observed in ^{174,176}Re [24,4] and in a series of odd-odd iridium isotopes [32] supporting the observation of such a band in ^{172}Re.

It should be noted that the rotational bands based on the configurations described above have been identified in many odd-odd nuclei in this region (for example, in ^{176}Re [4]). They are found to be strongly populated and easier to observe using heavy-ion-induced fusion-evaporation reactions and standard in-beam γ-ray spectroscopic techniques; this is consistent with our experimental observations. The three bands in ^{172}Re corresponds to a suppressed band (band 1), a semidecoupled band (band 2), and a doubly decoupled one (band 3). Our configuration assignments are further supported by the analyses of alignments, in-band decay properties, and signature splitting. These will be discussed in the following sections.

B. Alignment properties

In the standard cranked shell model analysis [31], the quasiparticle alignment of a rotational band can be expressed as

$$i_x(\omega) = I_x(\omega) - R(\omega), \tag{3}$$

with $I_x(\omega)$ the total aligned angular momentum along the rotation axis and $R(\omega)$ the collective contribution. The values of $I_x(\omega)$ and ω can be derived from the level spin I and the experimental level spacings

$$I_x(\omega) = \sqrt{(I+1/2)^2 - K^2}, \tag{4}$$

$$\hbar\omega = \frac{dE(I)}{dI_x(I)} \approx \frac{E(I+1)-E(I-1)}{I_x(I+1)-I_x(I-1)}, \tag{5}$$

and the collective component is parametrized using the Harris expression

$$R_x(\omega) = J_0\omega + J_1\omega^3, \tag{6}$$

where the Harris parameters J_0 and J_1 can be extracted using the method proposed by Drissi and co-workers [33].

Using Eqs. (3)–(6), we have extracted the experimental quasiparticle alignments i_x for the three bands in ^{172}Re (see Table II). Since the nuclear deformations (β_2, β_4, and γ) or pairing may be different for the different configurations [34], individual Harris parameters were used in order that the quasiparticle alignments are nearly constant for each band before first band crossing. For the reasons of systematic comparison, the same procedure has been applied to the related bands of neighboring odd-*A* nuclei. The Harris parameters used and the extracted i_x are also given in Table II. Figure 6 shows the plots of quasiparticle alignments i_x versus rotational frequency $\hbar\omega$.

An alignment of $6.6\hbar$ at $\hbar\omega=0.2$ MeV and a sharp upbend at $\hbar\omega=0.30$ MeV are observed for band 1 which has been assigned to be built on the two-quasiparticle configuration $\pi h_{11/2}(9/2^-[514])\otimes\nu i_{13/2}$. The $h_{11/2}(9/2^-[514])$ proton and the $i_{13/2}(5/2^+[642])$ neutron alignments are extracted to be $2.5\hbar$ from ^{171}Re and $5.1\hbar$ from ^{171}W (see Table II). According to the additivity rule in alignment [31], band 1 should have an initial alignment of $i_x(pn)=i_x(\pi h_{11/2})+i_x(\nu i_{13/2})\approx 2.5+5.1=7.6\hbar$ which is $1\hbar$ higher than the extracted value. This inconsistency may be due to improper choice of Harris parameters. Of course, if the level spins in band 1 were increased by one unit, the additivity rule in alignment [31] could be satisfied. This is unlikely since one unit increment in spins will change the level staggering phase; we shall discuss this

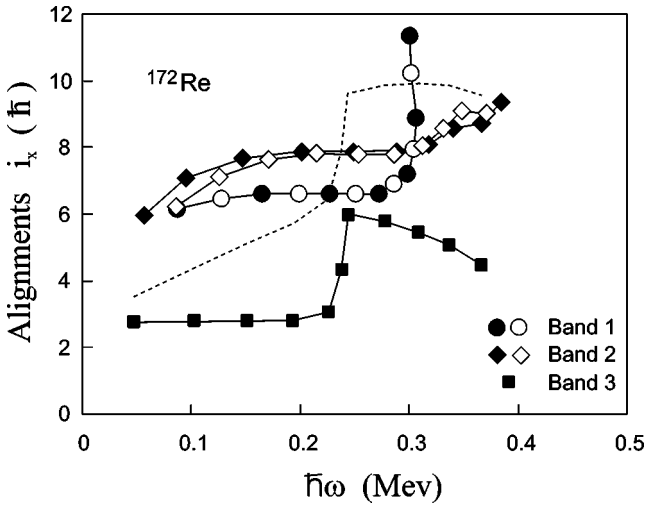

FIG. 6. Plot of quasiparticle alignments i_x vs $\hbar\omega$. Individual Harris parameters (J_0 and J_1 given in Table II) are used for each band. The dashed line represents the alignment for band 3 using the Harris parameters of band 1.

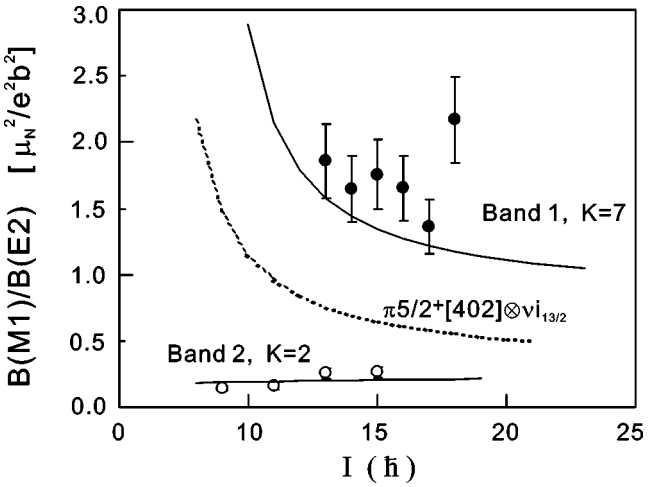

FIG. 7. Experimental $B(M1)/B(E2)$ ratios as a function of spin for band 1 (filled circles) and band 2 (open circles). The curves correspond to calculations using the geometric model of Dönau and Frauendorf [40].

problem in Sec. III D. The sudden upbend at $\hbar\omega_c$ =0.30 MeV corresponds to the neutron *BC* crossing expected for the $\pi h_{11/2}(9/2^-[514])\otimes\nu i_{13/2}$ configuration. The *BC* crossing occurs at $\hbar\omega$=0.31 MeV in the $\nu i_{13/2}$ band of ^{171}W. The slight reduction of *BC* crossing frequency in band 1 can be attributed to the small β and negative-γ driving effects of $h_{11/2}(9/2^-[514])$ orbital [35–37], thus enhancing the action of the Coriolis force on the pair of $i_{13/2}$ neutrons.

From Fig. 6, one can see that band 2 shows the highest initial alignments, and the backbend or upbend is apparently delayed with respect to band 1. This is consistent with our proposed spin and configuration assignments. As for the quasiparticle alignments, the $h_{9/2}$ proton and $i_{13/2}$ neutron contribute roughly $2.6\hbar$ and $5.1\hbar$ initial alignments, respectively (see Table II) leading to $i_x(pn)=i_x(\pi h_{9/2})+i_x(\nu i_{13/2})\approx 5.1+2.6=7.7\hbar$. This alignment value is very close to the extracted alignment in band 2: $i_x=7.8\hbar$ at $\hbar\omega$=0.20 MeV. The first band crossing in the ground-state band of ^{170}W occurs at $\hbar\omega_c$=0.25 MeV corresponding to the alignment of a pair of $i_{13/2}$ neutrons, i.e., the neutron *AB* crossing in the terminology of cranked shell model. This neutron *AB* crossing is blocked in band 2 with a quasineutron in the $i_{13/2}$ subshell. The backbend in band 2 will thus correspond to the neutron *BC* (and *AD*) crossing at higher rotational frequency. This *BC* (*AD*) crossing has been observed in ^{171}W at $\hbar\omega_c$ =0.31 MeV ($\hbar\omega_c$=0.35 MeV) as shown in Table II. However, no band crossing has been observed in band 2 up to the highest frequency measured. This can be attributed to the involvement of the $\pi h_{9/2}(1/2^-[541])$ proton. In fact, it has been well established [38] that band crossings in the $\pi h_{9/2}(1/2^-[541])$ bands of rare-earth nuclei are delayed with respect to their even-even neighbors due to the combined effects of shape driving effects [35–37] and the *p-n* residual interactions [4,13,39]. Such shape driving effects and residual *p-n* residual interactions still exist in the $\pi h_{9/2}(1/2^-[541])\otimes\nu i_{13/2}$ bands leading to the delayed *BC* (and *AD*) crossings in band 2. This phenomenon has been observed in a number of semidecoupled bands of this mass region [30] supporting our configuration assignment for band 2.

The first band crossings have been observed at $\hbar\omega_c$ =0.24 MeV for band 3. This is consistent with the configuration assignment of $\pi h_{9/2}(1/2^-[541])\otimes\nu 1/2^-[521]$. In this structure, the neutron *AB* crossing is allowed as observed at $\hbar\omega_c$=0.25 MeV in ^{170}W. The *AB* crossing in band 3 is slightly reduced. This could be understood as the combined effect of the $h_{9/2}(1/2^-[541])$ proton and the $1/2^-[521]$ neutron; the $h_{9/2}(1/2^-[541])$ proton induces a 20-keV delay and the $1/2^-[521]$ neutron causes 30-keV shift to lower rotational frequency as observed in ^{175}W [4]. The initial alignment is roughly $i_x\sim 2.8\hbar$, because of the smallest alignment ($\sim 0.5\hbar$) of the $1/2^-[521]$ neutron. Finally, Fig. 6 shows that the alignment gain for the *AB* crossing in band 3 is less than $4\hbar$ which is too small to be compared with the expected value of $6\rightarrow 8\hbar$ for the *AB* crossing in the ground-state bands of even-even neighbors. This may be due to the improper Harris parameters used for band 3. In fact, if the same Harris parameters as for band 1 is used, the alignment gain of $6.5\hbar$ can be obtained as the dashed line in Fig. 6. In this case, however, one has to explain the gradual alignment before $\hbar\omega$=0.23 MeV; this is beyond the scope of this paper.

C. $B(M1)/B(E2)$ ratios for bands 1 and 2

The in-band decay properties provide a sensitive test for configuration assignments. The experimentally extracted $B(M1)/B(E2)$ ratios for bands 1 and 2 are plotted in Fig. 7. Theoretical $B(M1)/B(E2)$ ratios have been estimated using the semiclassical formula developed by Dönau and Frauendorf [40]:

$$B(M1, I\rightarrow I-1)=\frac{3}{8\pi}[(g_p-g_R)A+(g_n+g_R)B]^2(\mu_N^2), \tag{7}$$

$$A = \left(1 - \frac{K^2}{I^2}\right)^{1/2} \Omega_p - i_p \frac{K}{I}, \quad (8)$$

$$B = \left(1 - \frac{K^2}{I^2}\right)^{1/2} \Omega_n - i_n \frac{K}{I}, \quad (9)$$

$$B(E2, I \rightarrow I-2) = \frac{5}{16\pi} \langle IK20|I-2K\rangle^2 Q_0^2 (e^2 b^2). \quad (10)$$

Here $g_{p(n)}$, $i_{p(n)}$, and $\Omega_{p(n)}$ represent the g factor, the alignment, and the projection angular momentum component on the symmetry axis of the proton (neutron) in the associated neighboring odd-mass nuclei. These values are taken from the compilation in Refs. [4,41] and presented in Table II. Q_0 is the intrinsic quadrupole moment of the nucleus, we take $Q_0 = 6.0\ eb$ which is close to the transition quadrupole moment of the ground-state band in ^{170}W [42]. A common collective g factor ($g_R = 0.3$) was used in the calculations. The calculated results are compared with experiment in Fig. 7 under the assumptions of $\pi h_{11/2}(9/2^-[514]) \otimes \nu i_{13/2}$ (band 1), $\pi h_{9/2}(1/2^-[541]) \otimes \nu i_{13/2}$ (band 2), and $\pi d_{5/2}(5/2^+[402]) \otimes \nu i_{13/2}$ configurations. It is apparent that the experimental $B(M1)/B(E2)$ ratios can be well reproduced supporting our spin and configuration assignments for bands 1 and 2. The $\pi d_{5/2}(5/2^+[402]) \otimes \nu i_{13/2}$ configuration has also a large g_K value and may form a compressed band [23] similar to band 1 at lower excitations. Theoretical calculations shown in Fig. 7 exclude this possibility due to its lower $B(M1)/B(E2)$ ratios predicted. The theoretical $B(M1)/B(E2)$ ratios are underestimated for band 1, this may be due to the fact that the experimental values are in fact the upper limits since the mixing ratios in Eq. (2) have been set to zero.

D. Signature inversion in the $\pi h_{11/2} \otimes \nu i_{13/2}$ band of ^{172}Re

Accepting the configuration and spin-parity assignments discussed in the previous sections, we analyzed the characteristics of signature splitting in band 1. Typical level staggering curves $S(I) = E(I) - E(I-1) - \frac{1}{2}[E(I+1) - E(I) + E(I-1) - E(I-2)]$ vs I are plotted on the left side in Fig. 8 for the $\pi h_{11/2} \otimes \nu i_{13/2}$ band in ^{172}Re. In such a plot, the points (associated with levels Is) that have negative values are energetically favored over those with positive ones. The expected favored signature is $\alpha_f = 0$ for the $\pi h_{11/2} \otimes \nu i_{13/2}$ configuration. It can be seen in this figure that at low spins, it is the $\alpha_{uf} = 1$ signature that is favored energetically rather than the $\alpha_f = 0$ sequence. Such behavior has been referred to as signature inversion or anomalous signature splitting [6]. With increasing angular momentum, the inverted signature splitting decreases, and the two signature branches cross with each other at $I_c = (18.5^-)$ beyond which normal signature splitting is observed.

Previous studies of odd-odd nuclei in this mass region have established a consistent pattern of signature splitting for a number of $\pi h_{11/2} \otimes \nu i_{13/2}$ bands. Systematic studies and analyses have been made in several recent publications (see, for example, Refs. [3,4,16,43]). For band 1 in ^{172}Re, the crossing spin is observed at $I_c = (18.5^-)$, which is two units higher than $I_c = (16.5^-)$ in ^{170}Ta [41,44] and three units higher than $I_c = (15.5^-)$ in ^{176}Re [4]. Furthermore, the inverted signature splitting in ^{172}Re is larger than that in the same band of its lower-Z isotone ^{170}Ta [41,44] and heavier isotope ^{176}Re [4]. These two features are consistent with systematic observations [4,43]. Different mechanisms have been proposed to interpret the low-spin signature inversion phenomenon using several theoretical approaches [2,6,12,14,16,45,46]. Here it may be worth noting that the proton Fermi surface in Ta, Re, and Ir isotopes lies in the vicinity of $\Omega = 9/2$ Nilsson orbital of $h_{11/2}$ subshell. The observations of signature inversion in ^{164}Ta [47], ^{172}Re (this work), ^{176}Re [4], and ^{178,180}Ir [5,32] indicate that the low-spin signature inversion exists in a wider range of nuclei than previously predicted [6,46] and the position of proton Fermi surface may not be a strict restriction to the presence of such a phenomenon.

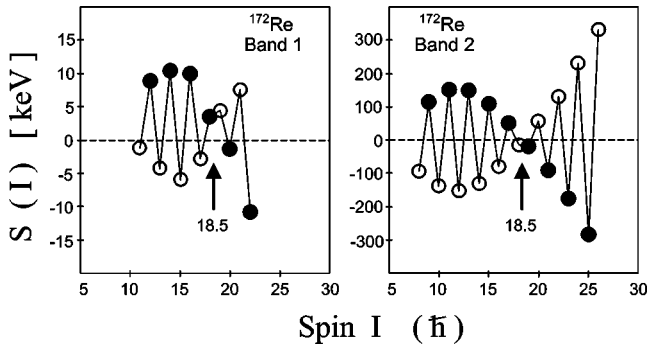

FIG. 8. Plot of signature splittings $S(I)$ vs I for the two-quasiparticle bands observed in ^{172}Re and the corresponding one-quasiparticle bands in neighboring ^{173}Re [20] and ^{173}W [29]. The filled (opened) symbols correspond to the signature-favored (signature-unfavored) levels. The arrows indicate the signature crossing spins.

E. Signature inversion in the $\pi h_{9/2} \otimes \nu i_{13/2}$ bands of ^{172}Re and neighbors

The level staggering curves $S(I)$ vs I is plotted on the right side in Fig. 8 for band 2 in ^{172}Re; the favored signature corresponds to $\alpha_f = 1$ for this $\pi h_{9/2} \otimes \nu i_{13/2}$ configuration. One can see that the $\alpha_{uf} = 0$ branch is energetically favored over that of $\alpha_f = 1$ at low spins. With increasing angular momentum, the anomalous signature splitting decreases, and the two signature branches cross each other at $I_c = (18.5^-)$ beyond which normal signature splitting is restored.

The low-spin signature inversion in the $\pi h_{9/2} \otimes \nu i_{13/2}$ semidecoupled bands was found by Bark and co-workers very recently in ^{162,164}Tm and ^{174}Ta [13]. Subsequently, a number of such bands have been reported to show the inversion phenomenon. Figure 9 shows the systematics of signature inversion in the $\pi h_{9/2} \otimes \nu i_{13/2}$ bands observed to date. With careful inspection of the signature inversion systematics shown in Fig. 9, one can draw the following conclusions.

(1) Low-spin signature inversion seems to exist in all the $\pi h_{9/2} \otimes \nu i_{13/2}$ bands of odd-odd nuclei in the $69 \leqslant Z \leqslant 79, 93 \leqslant N \leqslant 103$ region.

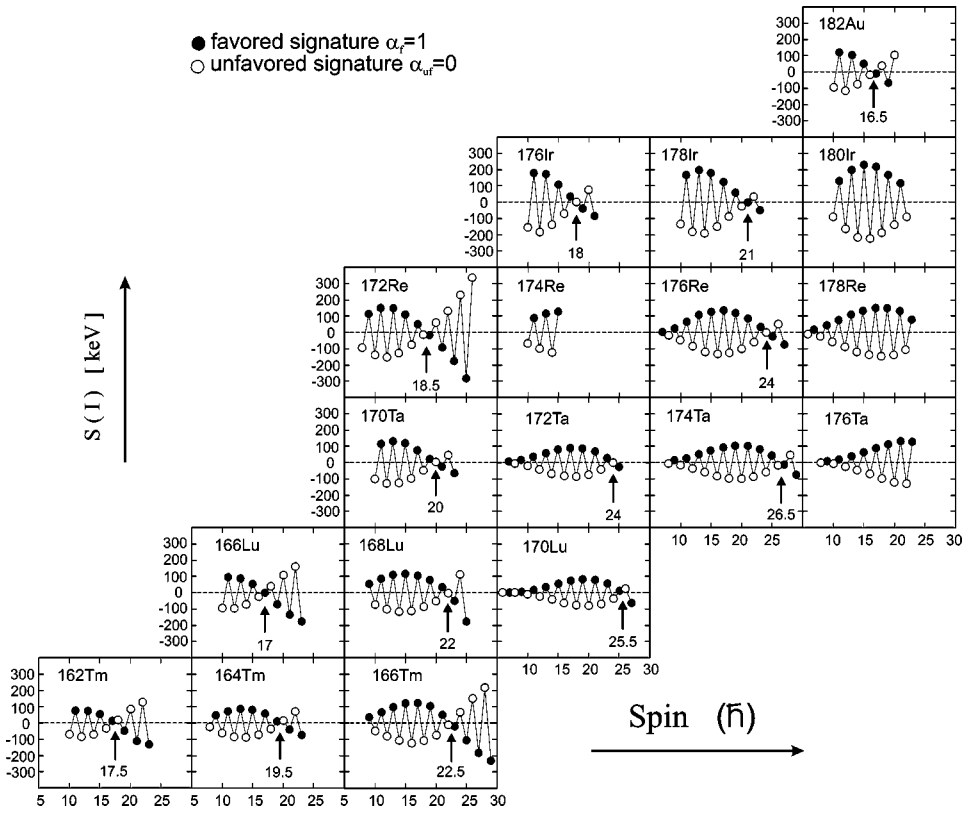

FIG. 9. A compilation of signature inversion for the $\pi h_{9/2} \otimes \nu i_{13/2}$ bands in $A=160\sim180$ mass region. The filled (opened) symbols correspond to the levels with favored signature $\alpha_f=1$ (unfavored signature $\alpha_{uf}=0$). The arrows indicate the signature crossing spins. The data sources are ^{182}Au [11], ^{176}Ir [10,49], ^{178}Ir [5,50], ^{180}Ir [32], ^{172}Re [this work], ^{174}Re [24], ^{176}Re [4], ^{178}Re [4,25], ^{170}Ta [41,44], ^{172}Ta [51], ^{174}Ta [13], ^{176}Ta [34], ^{166}Lu [52], ^{168}Lu [53,54], ^{170}Lu [43], ^{162,164}Tm [13], ^{166}Tm [55].

(2) For a chain of isotopes/isotones, the signature crossing spin I_c decreases with decreasing/increasing two neutrons/protons. This systematic behavior may explain the nonobservation of crossing spins in ^{176}Ta, ^{178}Re, and ^{180}Ir; their signature crossing spins are expected (see Fig. 9) to be the highest for each of the isotope chains.

(3) The systematic changes of I_c versus Z (or N) in the $\pi h_{9/2} \otimes \nu i_{13/2}$ bands are opposite to the trends in the $\pi h_{11/2} \otimes \nu i_{13/2}$ bands. In the latter case, the signature crossing spin increases $2\sim3\hbar$ with decreasing/increasing two neutrons/protons [3].

(4) The change in I_c in the $\pi h_{9/2} \otimes \nu i_{13/2}$ bands is less regular than that in the $\pi h_{11/2} \otimes \nu i_{13/2}$ bands. One can see in Fig. 9 that the inversion spin in ^{168}Lu is $22\hbar$ which is nearly the same as that in ^{166}Tm, while the inversion spin in ^{182}Au is at least $7\hbar$ lower than that of its isotone ^{180}Ir. This irregularity may be due to improper spin assignments, thus the systematic comparison could be more illuminating in the rotating frame by observing the crossing in Routhians (as suggested in Refs. [7,28]).

The low-spin signature inversion in band 2 of ^{172}Re and the crossing spin observed at $I_c=(18.5^-)$ are completely consistent with points (1)–(4), supporting our spin and configuration assignments. Usually the level spins in odd-odd nuclei are difficult to determine experimentally; one unit uncertainty still exists in spin assignment using level spacing systematics and the additivity rule of quasiparticle alignments. This may change the level staggering phase if the level spins are increased by one unit. Therefore, the observation of the crossing spin I_c at relatively higher spin levels provides an important argument for the low-spin signature inversion, since the Coriolis force which does not favor signature inversion, increases with frequency, it is much more likely that normal ordering will be observed at high spins versus low spins.

The two quasiparticle plus rotor model including *p-n* residual interaction has been applied recently to interpret the inversion phenomenon in the $\pi h_{9/2}(1/2^-[541]) \otimes \nu i_{13/2}$ bands of ^{162,164}Tm, ^{174}Ta, and ^{176}Re [2,4,13]; it has been determined that the proton-neutron residual interaction was necessary to produce the low-spin signature inversion. The extended total Routhians surface calculations showed that the quadrupole pairing plays a role in generating the low-spin signature inversion in the $\pi h_{9/2} \otimes \nu i_{13/2}$ band of ^{182}Au [11]. It seems that both theoretical approaches give reasonable descriptions of signature inversion for some selected cases. In this sense, a reproduction of systematic trends of points (1)–(4) may be crucial for a full understanding of signature inversion in the $\pi h_{9/2} \otimes \nu i_{13/2}$ bands.

Cardona and co-workers [4] have investigated the signature inversion in the $\pi h_{9/2}(1/2^-[541]) \otimes \nu i_{13/2}$ band of ^{176}Re using a two quasiparticle plus rotor model including *p-n* residual interaction. Using a weak coupling basis, they found that a large repulsive matrix element of the *p-n* force acts in the maximally aligned intrinsic state $J=j_\pi+j_\nu=11$, so that the role of $J=10$ component is dominant at low-spin states. This leads to the favored states of $I=R+J=R+10=$*even* and the unfavored states of $I-1=R+10-1=$*odd* ($R=$even is the well defined core angular momentum). The authors of Ref. [4] claimed that only when the rotational energy required to go from one state to the next one starts to become comparable to the intrinsic (*p-n* interaction) energy required to maximally align proton and neutron (to $J=11$) will the change of phase occur. According to this theoretical explanation and the well-

known formula of $E(I-2\rightarrow I)=(\hbar^2/2\mathcal{I})(4I-2)\propto(4I-2)/A^{7/3}\beta^2$, a critical spin can be expressed as $I_c\propto E(I_c-2\rightarrow I_c)A^{7/3}\beta^2$. Assuming that the rotational energy $E(I_c-2\rightarrow I_c)$ used to maximally align proton and neutron (to $J=11$) keeps constant in the mass region of interest, the critical spin I_c will decrease with decreasing A and β. Actually, theoretical calculations have shown that the ground-state quadrupole deformations of corresponding even-even cores of Er through Pt decrease with decreasing N [48]; this may be related to the experimental observations that the signature crossing spin decreases with decreasing N in a given isotopic chain. The fact that the signature crossing spin decreases with increasing Z in a given isotonic chain (see Fig. 9) may be explained, at least qualitatively, by decreasing the quadrupole deformations of the respective cores [48] (the relative increase in A is much smaller than the decrease in β). A close inspection of Fig. 9 and Fig. 2 in Ref. [48] seems to reveal that there exist certain correlations between the regularity of crossing spin and the nuclear deformations (mainly β). Finally, it is worth noting that the nearly constant amplitude in signature splitting is observed in Fig. 9. This is in contrast to the $\pi h_{11/2}\otimes\nu i_{13/2}$ bands (Ref. [3]) and the $\pi h_{11/2}\otimes\nu h_{11/2}$ bands (Ref. [28]) where distinct trends in amplitude are observed. In fact, the bands shown in Fig. 9 correspond to the $\pi h_{9/2}(\alpha_f=1/2)\otimes\nu i_{13/2}(\alpha=\pm1/2)$ configuration, that is, the $h_{9/2}$ proton contributes a favored signature while both favored and unfavored signatures are involved for the $i_{13/2}$ neutron. Thus the signature splitting in a $\pi h_{9/2}(\alpha_f=1/2)\otimes\nu i_{13/2}(\alpha=\pm1/2)$ band could be due to the $i_{13/2}$ neutron, and the amplitude of signature splitting depends on the distance of neutron Fermi surface to the $\nu 1/2^+[660](i_{13/2})$ Nilsson orbital. The nearly constant amplitude in signature splitting observed in Fig. 9 deviates from an expectation that the signature splitting decreases with increasing N. This is in need of further investigations.

IV. CONCLUSIONS

In conclusion, an in-beam γ-spectroscopy experiment has been performed leading to the first observation of three rotational bands in odd-odd ^{172}Re. The quasiparticle configurations and the level spin assignments for each band have been made on the basis of several considerations such as quasiparticle alignments, signature splitting, in-band electromagnetic transition properties, level spacing systematics, band crossings, etc. The signature inversion in the $\pi h_{9/2}\otimes\nu i_{13/2}$ and $\pi h_{11/2}\otimes\nu i_{13/2}$ bands have been established due to the observation of a signature crossing at $I\sim18.5\hbar$, extending our knowledge on signature inversion to the lightest neutron deficient odd-odd rhenium isotope. The systematics of signature inversion in the $\pi h_{9/2}\otimes\nu i_{13/2}$ bands in $A=160\sim180$ mass region are presented and some general features are discussed with reference to the theoretical calculations of two Quasiparticle plus rotor model including p-n interactions. Accepting the transparent picture described by Cardona and co-workers, the regularity in signature crossing spin seems to be closely related to the nuclear quadrupole deformation.

ACKNOWLEDGMENTS

The authors wish to thank the staffs in the JAERI tandem accelerator for providing ^{27}Al beam and their hospitality during experiment. This work was partially supported by the National Natural Sciences Foundation of China (Grant Nos. 10025525 and 1005012), the Chinese Academy of Sciences, and the Major State Basic Research Development Program of China (Contract No. G2000077400). F.R.X. also acknowledges the support from the National Natural Sciences Foundation of China (Grant No. 10175002) and the Chinese Ministry of Education.

[1] A. Bohr and B. R. Mottelson, *Nuclear Structure* (Benjamin Inc., MA, 1975), Vol. 2.

[2] L. L. Riedinger, H. Q. Jin, W. Reviol, J.-Y. Zhang, R. A. Bark, G. B. Hagemann, and P. B. Semmes, Prog. Part. Nucl. Phys. **38**, 251 (1997).

[3] Y. Liu, Y. Ma, H. Yang, and S. Zhou, Phys. Rev. C **52**, 2514 (1995).

[4] M. A. Cardona, A. J. Kreiner, D. Hojman, G. Levinton, M. E. Debray, M. Davidson, J. Davidson, R. Pirchio, H. Somacal, D. R. Napoli, D. Bazzacco, N. Blasi, R. Burch, D. De Acuna, S. M. Lenzi, G. Lo Bianco, J. Rico, and C. Rossi Alvarez, Phys. Rev. C **59**, 1298 (1999).

[5] Y. H. Zhang, T. Hayakawa, M. Oshima, Y. Toh, J. Katakura, Y. Hatsukawa, M. Matsuda, N. Shinohara, T. Ishii, H. Kusakari, M. Sugawara, and T. Komatsubara, Eur. Phys. J. A **8**, 439 (2000).

[6] R. Bengtsson, H. Frisk, R. F. May, and J. A. Pinston, Nucl. Phys. **A415**, 189 (1984).

[7] G. García Bermúdez and M. A. Cardona, Phys. Rev. C **64**, 034311 (2001).

[8] D. Hojman, M. A. Cardona, D. R. Napoli, S. M. Lenzi, C. A. Ur, G. Lo Bianco, C. M. Petrache, M. Axiotis, D. Bazzacco, J. Davidson, M. Davidson, M. De Poli, G. de Angelis, E. Farnea, T. Kroell, S. Lunardi, N. Marginean, T. Martinez, R. Menegazzo, B. Quintana, and C. Rossi Alvarez, Eur. Phys. J. A **10**, 245 (2001).

[9] Y. H. Zhang, T. Hayakawa, M. Oshima, Y. Toh, J. Katakura, Y. Hatsukawa, M. Matsuda, N. Shinohara, T. Ishii, H. Kusakari, M. Sugawara, T. Komatsubara, and K. Furuno, Chin. Phys. Lett. **18**, 1323 (2001).

[10] Y. H. Zhang, M. Oshima, Y. Toh, M. Koizumi, A. Ossa, T. Shizuma, T. Hayakawa, M. Sugawara, H. Kusakari, T. Morikawa, S. X. Wen, and L. H. Zhu, Eur. Phys. J. A **13**, 429 (2002).

[11] Y. H. Zhang, F. R. Xu, J. J. He, Z. Liu, X. H. Zhou, Z. G. Gan, T. Hayakawa, M. Oshima, T. Toh, T. Shizuma, J. Katakura, Y. Hatsukawa, M. Matsuda, H. Kusakari, M. Sugawara, K. Furuno, T. Komatsubara, T. Une, S. X. Wen, and Z. M. Wang, Eur. Phys. J. A **14**, 271 (2002).

[12] P. B. Semmes and I. Ragnarsson, *Proceedings of International*

Conference on High-Spin Physics and Gamma-Soft Nuclei, Pittsburgh, PA, 1990, edited by J. X. Saladin, R. A. Sorensen, and C. M. Vincent (World Scientific, Singapore, 1991), p. 500.
[13] R. A. Bark, J. M. Espino, W. Reviol, P. B. Semmes, H. Carlsson, I. G. Bearden, G. B. Hagemann, H. J. Jensen, I. Ragnarsson, L. L. Riedinger, H. Ryde, and P. O. Tjom, Phys. Lett. B **406**, 193 (1997).
[14] K. Hara and Y. Sun, Nucl. Phys. **A531**, 221 (1991).
[15] A. K. Jain and A. Goel, Phys. Lett. B **277**, 233 (1992).
[16] F. R. Xu, W. Satula, and R. Wyss, Nucl. Phys. **A669**, 119 (2000).
[17] C. Plettner, I. Ragnarsson, H. Schnare, R. Schwengner, L. Käubler, F. Dönau, A. Algora, G. de Angelis, D. R. Napoli, A. Gadea, J. Eberth, T. Steinhardt, O. Thelen, M. Hausmann, A. Müller, A. Jungclaus, K. P. Lieb, D. G. Jenkins, R. Wadsworth, and A. N. Wilson, Phys. Rev. Lett. **85**, 2454 (2000).
[18] B. Singh, Nucl. Data Sheets **75**, 199 (1995).
[19] K. Furuno, M. Oshima, T. Komatsubara, K. Furutaka. T. Hayakawa, M. Kidera, Y. Hatsukawa, M. Matsuda, S. Mitarai, T. Shizuma, T. Saitoh, N. Hashimoto, H. Kusakari, M. Sugawara, and T. Morikawa, Nucl. Instrum. Methods Phys. Res. A **421**, 211 (1999).
[20] R. A. Bark, G. D. Dracoulis, A. E. Stuchbery, A. P. Byrne, A. M. Baxter, F. Riess and P. K. Weng, Nucl. Phys. **A501**, 157 (1989).
[21] J. Espino, J. D. Garrett, G. B. Hagemann, P. O. Tjom, C.-H. Yu, M. Bergstrom, L. Carlen, L. P. Ekstrom, J. Lyttkens-Linden, H. Ryde, R. Bengtsson, T. Bengtsson, R. Chapman, D. Clarke, F. Khazaie, J. C. Lisle, and J. N. Mo, Nucl. Phys. **A567**, 377 (1994).
[22] S. G. Li, S. Wen, G. J. Yuan, G. S. Li, P. F. Hua, L. K. Zhang, Z. K. Yu, P. S. Yu, P. K. Weng, C. X. Yang, R. Chapman, D. Clarke, F. Khazaie, J. C. Lisle, J. N. Mo, J. D. Garrett, G. B. Hagemann, B. Herskind, and H. Ryde, Nucl. Phys. **A555**, 435 (1993).
[23] A. J. Kreiner, J. Davidson, M. Davidson, D. Abriola, C. Pomar, and P. Thieberger, Phys. Rev. C **36**, 2309 (1987); **37**, 1338 (1988).
[24] Y. H. Zhang, S. Q. Zhang, W. X. Huang, X. H. Zhou, X. C. Feng, X. Xu, X. G. Lei, Y. X. Guo, S. F. Zhu, J. J. He, Z. Liu, S. J. Wang, and Y. X. Luo, Eur. Phys. J. A **7**, 19 (2000).
[25] A. J. Kreiner, V. R. Vanin, F. A. Beck, Ch. Bourgeois, Th. Byrski, D. Curien, G. Duchene, B. Haas, J. C. Merdinger, M. G. Porquet, P. Romain, S. Rouabah, D. Santos, and J. P. Vivien, Phys. Rev. C **40**, R487 (1989).
[26] A. J. Kreiner, D. E. Di Gregorio, A. J. Fendrik, J. Davidson, and M. Davidson, Phys. Rev. C **29**, 1572 (1984).
[27] Y. Liu, J. Lu, Y. Ma, S. Zhou, and H. Zheng, Phys. Rev. C **54**, 719 (1996).
[28] D. J. Hartley, L. L. Riedinger, M. Danchev, W. Reviol, O. Zeidan, J.-Y. Zhang, A. Galindo-Uribarri, C. J. Gross, C. Baktash, M. Lipoglavsek, S. D. Paul, D. C. Radford, C.-H. Yu, D. G. Sarantites, M. Devlin, M. P. Carpenter, R. V. F. Janssens, D. Seweryniak, and E. Padilla, Phys. Rev. C **65**, 044329 (2002).
[29] P. M. Walker, G. D. Dracoulis, A. Johnston, J. R. Leigh, M. G. Slocombe, I. F. Wright, J. Phys. G **4**, 1655 (1978).
[30] A. J. Kreiner, Nucl. Phys. **A520**, 225c (1990).
[31] R. Bengtsson and S. Frauendorf, Nucl. Phys. **A314**, 27 (1979); **A327**, 139 (1979).
[32] Y. H. Zhang, T. Hayakawa, M. Oshima, J. Katakura, Y. Hatsukawa, M. Matsuda, H. Kusakari, M. Sugawara, T. Komatsubara, and K. Furuno, Phys. Rev. C **65**, 014302 (2002).
[33] S. Drissi, A. Bruder, J.-Cl. Dousse, V. Ionescu, J. Kern, J.-A. Pinston, S. André, D. Barnéoud, J. Genevey, and H. Frisk, Nucl. Phys. **A451**, 313 (1986).
[34] F. G. Kondev, G. D. Dracoulis, A. P. Byrne, and T. Kibedi, Nucl. Phys. **A632**, 473 (1998).
[35] S. Frauendorf, Phys. Scr. **T24**, 349 (1981).
[36] C.-H. Yu, G. B. Hagemann, J. M. Espino, K. Furuno, J. D. Garrett, R. Chapman, D. Clarke, F. Khazaie, J. C. Lisle, J. N. Mo, M. Bergstrom, L. Carlen, P. Ekstrom, J. Lyttkens, and H. Ryde, Nucl. Phys. **A511**, 157 (1990).
[37] L. L. Riedinger, H.-Q. Jin, and C.-H. Yu, Nucl. Phys. **A520**, 287c (1990).
[38] H. J. Jensen, R. A. Bark, R. Bengtsson, G. B. Hagemann, P. O. Tjøm, S. Y. Araddad, C. W. Beausang, R. Chapman, J. Copnell, A. Fitzpatrick, S. J. Freeman, S. Leoni, J. C. Lisle, J. Simpson, A. G. Smith, D. M. Thompson, S. J. Warburton, and J. Wrzesinski, Z. Phys. A **359**, 127 (1997).
[39] R. A. Bark, H. Carlsson, S. J. Freeman, G. B. Hagemann, F. Ingebretsen, H. J. Jensen, T. Lonnroth, M. J. Piiparinen, I. Ragnarsson, H. Ryde, H. Schnack-Petersen, P. B. Semmes, and P. O. Tjøm, Nucl. Phys. **A630**, 603 (1998).
[40] F. Dönau, Nucl. Phys. **A471**, 469 (1987); F. Dönau and S. Frauendorf, *Proceedings of the Conference on High Angular Momentum Properties of Nuclei*, Oak Ridge, TN, edited by N. R. Johnson (Harwood Academic, Chur, Switzerland, 1982), p. 143.
[41] Y. H. Zhang, S. Q. Zhang, Q. Z. Zhao, S. F. Zhu, H. S. Xu, X. H. Zhou, Y. X. Guo, X. G. Lei, J. Lu, Q. B. Gou, H. J. Jin, Z. Liu, Y. X. Luo, X. F. Sun, Y. T. Zhu, X. G. Wu, S. X. Wen, and C. X. Yang, Phys. Rev. C **60**, 044311 (1999).
[42] F. K. McGowan, N. R. Johnson, M. N. Rao, C. Baktash, I. Y. Lee, J. C. Wells, M. Kortelahti, and V. P. Janzen, Nucl. Phys. **A580**, 335 (1994).
[43] G. Levinton, A. J. Kreiner, M. A. Cardona, M. E. Debray, D. Hojman, J. Davidson, G. Marti, A. Burlon, M. Davidson, D. R. Napoli, M. De Poli, D. Bazzacco, N. Blasi, S. M. Lenzi, G. Lo Bianco, C. Rossi Alvarez, and V. R. Vanin, Phys. Rev. C **60**, 044309 (1999).
[44] Fu-Guo Deng, Chun-Xiang Yang, Hui-Bin Sun, Xiao-Guang Wu, Jing-Bin Lu, Guang-Yi Zhao, Guang-Bing Han, Zhao-Hua Peng, Li-Chang Yin, Shu-Xian Wen, Guang-Sheng Li, Guan-Jun Yuan, Hong-Yu Zhou, Yun-Zuo Liu, and Li-Hua Zhu, Chin. Phys. Lett. **18**, 888 (2001).
[45] Renrong Zheng, Shunquan Zhu, and Yunwei Pu, Phys. Rev. C **56**, 175 (1997).
[46] I. Hamamoto, Phys. Lett. B **235**, 221 (1990).
[47] D. G. Roux, E. Gueorguieva, B. R. S. Babu, D. G. Aschman, M. Benatar, R. Fearick, M. S. Fetea, J. J. Lawrie, G. K. Mabala, S. M. Mullins, S. H. T. Murray, S. Naguleswaran, R. T. Newman, C. Rigollet, J. F. Sharpey-Schafer, F. D. Smit, W. J. Whittaker, and R. A. Wyss, Phys. Rev. C **65**, 014308 (2002).
[48] R. Bengtsson, S. Frauendorf, and F.-R. May, At. Data Nucl. Data Tables **35**, 15 (1986).
[49] R. A. Bark, A. M. Baxter, A. P. Byrne, P. M. Davidson, G. D. Dracoulis, S. M. Mullins, T. R. McGoram, and R. T. Newman.

Phys. Rev. C **67**, 014320 (2003).

[50] D. Hojman, M. A. Cardona, D. R. Napoli, S. M. Lenzi, J. Davidson, M. Davidson, C. A. Ur, G. Lo Bianco, C. M. Petrache, M. Axiotis, D. Bazzacco, M. De Poli, G. de Angelis, E. Farnea, T. Kroell, S. Lunardi, N. Marginean, T. Martinez, R. Menegazzo, B. Quintana, and C. R. Alvarez, Phys. Rev. C **67**, 024308 (2003).

[51] D. Hojman, M. A. Cardona, M. Davidson, M. E. Debray, A. J. Kreiner, F. Le Blanc, A. Burlon, J. Davidson, G. Levinton, H. Somacal, J. M. Kesque, F. Naab, M. Ozafran, P. Stoliar, M. Vazquez, D. R. Napoli, D. Bazzacco, N. Blasi, S. M. Lenzi, G. Lo Bianco, and C. Rossi Alvarez, Phys. Rev. C **61**, 064322 (2000).

[52] G. Zhao, Y. Liu, J. Lu, Y. Ma, L. Yin, X. Li, Z. Li, X. Wu, G. Li, S. Wen, and C. Yang, Eur. Phys. J. A **9**, 299 (2000).

[53] S. K. Katoch, S. L. Gupta, S. C. Pancholi, D. Mehta, S. Malik, G. Shanker, L. Chaturvedi, and R. K. Bhowmik, Eur. Phys. J. A **4**, 307 (1999).

[54] S. X. Wen (unpublished).

[55] M. A. Cardona, D. Hojman, M. E. Debray, A. J. Kreiner, M. Davidson, J. Davidson, D. R. Napoli, D. Bazzacco, N. Blasi, S. M. Lenzi, G. Lo Bianco, and C. Rossi Alvarez, Phys. Rev. C **66**, 044308 (2002).